The Journal of Chemical Physics

RESEARCH ARTICLE | MARCH 02 2026

High-resolution optical spectroscopy of buffer-gas-cooled silicon monofluoride ($^{28}Si^{19}F$)

Jie Ma; Yuxi Feng ; Yemin Pan; Shanwu Wang; Rui Li; Zesen Wang ; Shunyong Hou; Xilin Bai; Xiaohu Li ; Liang Xu ; Xingjia Li; Zhenghai Yang ; Jianping Yin; Tao Yang

J. Chem. Phys. 164, 094304 (2026)
https://doi.org/10.1063/5.0314009

AIP Publishing

The Journal of Chemical Physics ARTICLE pubs.aip.org/aip/jcp

High-resolution optical spectroscopy of buffer-gas-cooled silicon monofluoride ($^{28}Si^{19}F$)

Cite as: J. Chem. Phys. 164, 094304 (2026); doi: 10.1063/5.0314009
Submitted: 26 November 2025 • Accepted: 16 February 2026 •
Published Online: 2 March 2026

Jie Ma,[1] Yuxi Feng,[1] Yemin Pan,[1] Shanwu Wang,[1] Rui Li,[1] Zesen Wang,[1] Shunyong Hou,[1] Xilin Bai,[1] Xiaohu Li,[2,3,4] Liang Xu,[5] Xingjia Li,[6] Zhenghai Yang,[1,7,a)] Jianping Yin,[1] and Tao Yang[1,2,7,a)]

AFFILIATIONS

[1] State Key Laboratory of Precision Spectroscopy, East China Normal University, Shanghai 200062, China
[2] Xinjiang Astronomical Observatory, Chinese Academy of Sciences, 150 Science 1-Street, Urumqi, Xinjiang 830011, China
[3] Xinjiang Key Laboratory of Radio Astrophysics, 150 Science 1-Street, Urumqi, Xinjiang 830011, China
[4] Key Laboratory of Radio Astronomy and Technology, Chinese Academy of Sciences, A20 Datun Road, Chaoyang District, Beijing 100101, China
[5] Shanghai Key Lab of Modern Optical System, University of Shanghai for Science and Technology, 516 Jungong Road, Shanghai 200093, China
[6] School of Mathematics, Physics and Statistics, Shanghai University of Engineering Science, Shanghai 201620, China
[7] Collaborative Innovation Center of Extreme Optics, Shanxi University, Taiyuan, Shanxi 030006, China

[a)] **Authors to whom correspondence should be addressed:** zhyang@lps.ecnu.edu.cn and tyang@lps.ecnu.edu.cn

ABSTRACT

Precise measurement of high-resolution molecular spectroscopy plays an important role in elucidating the quantum nature governing the molecular properties and in exploring fundamental physics and chemistry. Here, we report the high-resolution optical spectroscopy of buffer-gas-cooled silicon monofluoride ($^{28}Si^{19}F$, hereafter SiF) molecules in the $A\ ^2\Sigma^+\ (v' = 0) \leftarrow X\ ^2\Pi_{1/2}\ (v = 0)$ transition. We measured a total of 94 hyperfine-resolved transitions with an uncertainty of 13.8 MHz via the laser-induced fluorescence technique, enabling the first determination of the hyperfine constant b and dipole–dipole interaction constant c of the $A\ ^2\Sigma^+$ state arising from the ^{19}F. By employing an effective Hamiltonian analysis, we reconstructed the hyperfine energy level structures for both ground and excited states, providing a comprehensive spectroscopic framework for SiF. These results establish SiF as a promising candidate for laser cooling, though the measured hyperfine splitting suggests that multiple frequency components will be required to achieve efficient optical cycling. Our findings enrich the spectroscopic database for cold SiF molecules, advancing their potential applications in quantum control, precision measurement, astrophysics, and plasma physics.

I. INTRODUCTION

The study of silicon monofluoride (SiF) holds significance in the fields of fundamental molecular physics, chemical vapor deposition (CVD), plasma physics, molecular collision dynamics, and astrophysics. In fluorinated CVD of silicon carbide, SiF has been identified as the dominant species in silicon growth, while SiHF acts as a minor contributor to the film formation process, highlighting the central chemical role of SiF in Si–C bond formation.[1] SiF molecules are also commonly observed in plasma environments during the etching and sputtering of silicon-containing semiconductor materials.[2–5] In electronically inelastic collisions, studies on SiF have shown that the energy disposal is governed by its electronic structure and the coupling among its excited states, underscoring that precise spectroscopic characterization is essential for understanding the underlying energy-transfer dynamics.[6–8] Furthermore, SiF has been detected in M-type stars,[9] and intensity distribution in the spectra is of interest in astrophysics and is necessary for an understanding of the evolutionary stages of emitting sources.[10] Therefore, investigating the molecular properties of SiF is of great significance, including its molecular geometry[11–14] and dissociation energy.[15–17] In particular, spectroscopic constants of SiF, as a vital branch of structural research, play an important role in elucidating its fundamental physicochemical properties.

For spectroscopic experiments, the band spectrum of SiF has been documented since 1958, including vibrational and rotational constants associated with its multiple electronic states.[18] In the 1970s, the $a\ ^4\Sigma^- \leftarrow X\ ^2\Pi$ electronic transition was recorded and assigned,[19] and the radiative lifetime of the $A\ ^2\Sigma^+$ state for SiF was measured for the first time.[20] Subsequent investigations have also been conducted on the higher excited states, including $B\ ^2\Sigma^+$, $C\ ^2\Delta$, and $E\ ^2\Pi$,[21,22] with particular attention given to studies pertaining to the Rydberg states.[23–26] For the ground state, the microwave spectrum of SiF and the molecular constants of the $X\ ^2\Pi$ state were reported.[18,27–29] On the theoretical side, in 1971, *ab initio* Hartree–Fock calculations established the ground-state electronic configuration and polarity of SiF.[13] Subsequent configuration interaction studies refined the ordering and bonding characteristics of its low lying valence states.[30] Later, high level CASSCF/MRCI +Q calculations incorporating core valence correlation and relativistic effects have accurately reproduced experimental spectroscopic constants, providing a reliable theoretical foundation for precise spectroscopic characterization of SiF.[31]

In recent years, alkaline-earth monofluorides, such as MgF,[32] AlF,[33] CaF,[34] SrF,[35] BaF,[36] YbF,[37] RaF,[38] and HgF,[39] have demonstrated unique advantages for laser cooling and precision measurements.[37,39–42] All of these above-mentioned molecules possess a Σ ground state. Recently, the laser cooling feasibility of SiF has been tentatively explored,[43] predicting that the $A\ ^2\Sigma^+\ (v' = 0) \leftarrow X\ ^2\Pi\ (v = 0)$ transition possesses a short radiative lifetime ($\approx$0.69 μs) and highly diagonal Franck–Condon factors ($R_{00} \approx 0.994$). These results suggest that SiF might be one of the promising candidates fulfilling key requirements for efficient optical cycling of laser cooling with a $^2\Pi$ ground state. However, investigations into the hyperfine structures of SiF needed for the design of the precision measurement schemes, such as the nearly closed transitions, have still remained elusive. Accounting for the natural isotopic abundances of silicon [^{28}Si (92.2%), ^{29}Si (4.7%), and ^{30}Si (3.1%)][44] and the fact that ^{19}F is the only stable isotope of fluorine, it is imperative to investigate first the high-resolution optical spectroscopy of $^{28}Si^{19}F$ (hereafter SiF). This strategy has also been adopted in the resonance enhanced multiphoton ionization (REMPI) study on SiF produced in a SiF_4 plasma, in which SiF ions were detected in the time of flight mass spectrometry (TOFMS).[45]

In this work, the buffer-gas-cooled SiF molecules are produced, and the high-resolution laser-induced fluorescence (LIF) spectra of the $A\ ^2\Sigma^+ \leftarrow X\ ^2\Pi_{1/2}$ transition are investigated. Using a continuous-wave laser, we recorded 94 fluorescence spectra of the $A\ ^2\Sigma^+\ (v' = 0) \leftarrow X\ ^2\Pi_{1/2}\ (v = 0)$ transition and resolved its hyperfine structures. By fitting and assigning these spectra, we determined the molecular constants of the $A^2\Sigma^+$ state and, for the first time, reported the ^{19}F hyperfine constant b and dipole–dipole interaction constant c for low-J levels. To provide a more intuitive understanding of the energy level structures of the $X\ ^2\Pi_{1/2}$ and $A\ ^2\Sigma^+$ states, we further calculated their hyperfine-resolved structures using the effective Hamiltonian approach. These results establish a spectroscopic basis for future laser cooling evaluations utilizing SiF. Overall, our findings enrich the spectroscopic database of SiF and provide a deeper understanding of its molecular properties, which will be of interest to the astrophysical, molecular spectroscopy, and precision measurement communities from a fundamental point of view.

II. EXPERIMENT

The schematic setup of our experiment has been described elsewhere[46] and is shown in Fig. 1. In brief, SiF molecules were generated in a buffer gas cell attached to the 5.5 ± 0.5 K cold plate of a pulse-tube cryocooler (Cryomech PT415). A silicon rod, mounted on a stepper motor providing a helical motion to ensure uniform ablation across the target surface, was ablated by the 532 nm second-harmonic output of a Nd:YAG laser [Continuum Surelite II (SLII-10), 2 Hz, 20 mJ per pulse]. The ablated silicon plasma reacted with a continuous flow of CF_4 introduced into the cell at a rate of 0.1 SCCM to form SiF molecules. These newly produced SiF molecules were subsequently cooled through collisions and thermalization with precooled helium buffer gas flowing at 2.0 SCCM. The base pressure in the source chamber reached 1.5×10^{-7} Pa (1.5×10^{-9} mbar) and increased to 3.0×10^{-4} Pa (3.0×10^{-6} mbar)

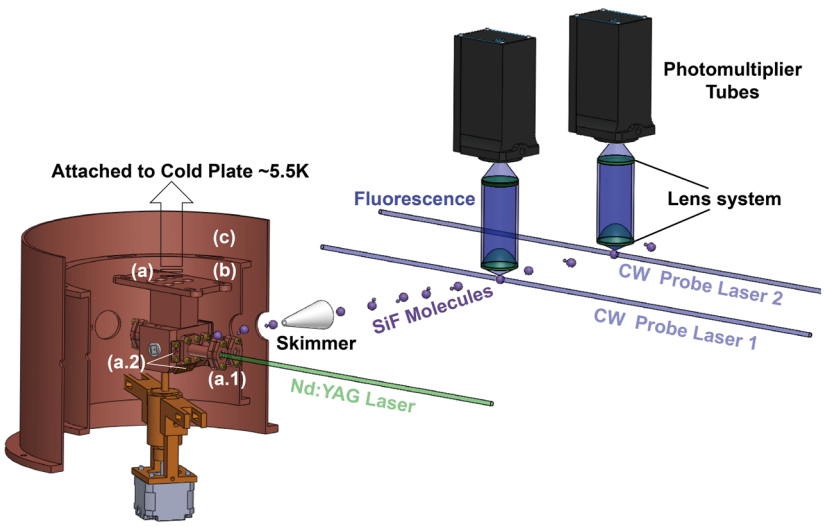

FIG. 1. Schematic diagram of the buffer gas cooling apparatus used for the laser-induced fluorescence (LIF) detection of SiF. (a) Buffer gas cooling cell attached to the cold plate held at ~5.5 K. (a.1) The laser ablation aperture (left) and the detection aperture (right). (a.2) The He gas inlet (top) and the CF_4 gas inlet (bottom). (b) First layer heat shield coated with activated carbon in the inner surface. (c) Second layer heat shield.

under experimental conditions with the buffer gas and ablation laser in operation. The resulting SiF beam exited the buffer gas cell and passed sequentially through the secondary heat shield (coated with activated charcoal), the primary heat shield, and a skimmer before entering the detection chamber, where the pressure was maintained at 2.0×10^{-6} Pa (2.0×10^{-8} mbar).

For the LIF detection, the 874 nm output of a continuous-wave laser (Toptica TA-SHG Pro) was calibrated via a high-precision wavemeter (WSU-30) and frequency-doubled to ~437 nm (1.5 mW/cm^2) in order to investigate the $A\,^2\Sigma^+$ ($v' = 0$) ← $X\,^2\Pi_{1/2}$ ($v = 0$) transition in the range of 685 488 680–685 687 560 MHz (22 865.44–22 872.08 cm^{-1}). The SiF beam intersected the first and second detection laser beams at 343 and 406 mm, respectively, downstream from the ablation point. The resulting fluorescence signals were collected by photomultiplier tubes (Hamamatsu H10721-113 and H3695-10) equipped with an optimized light collection lens system composed of an aspherical lens of 16 mm focal length and a plano-convex lens of 100 mm focal length to maximize the solid angle of collection, thus enhancing detection efficiency. The dual-channel acquisition card (NI PCI-5122) was synchronized with the Q-switch trigger of the Nd:YAG laser to digitize the fluorescence signals detected at two locations.

In addition, a photodetector (Thorlabs PDA25K2) was placed 343 mm downstream from the first detection beam to monitor its intensity, ensuring stable laser output throughout the experiment and maintaining high laser output, which is above the saturation absorption intensity of SiF. According to the fluorescence saturation formula [Eq. (1)] where I is the laser intensity, I_f is the fluorescence intensity, and $I_{f,max}$ is the saturation fluorescence intensity,[47] $I_f \approx I_{f,max}$ when $I \gg I_f$, implying that the impact of fluctuations in laser intensity on fluorescence intensity is significantly reduced. The saturation absorption intensity I_{sat} for SiF of the $A\,^2\Sigma^+$ state can be calculated using Eq. (2),[48] where h is Planck's constant, λ is the transition wavelength, and τ_s is the saturation time constant. For a simple two-level atom with a natural linewidth Γ, the saturation time constant $\tau_s = \Gamma^{-1}$,

$$I_f = I_{f,\max}\frac{I}{I + I_{sat}}, \tag{1}$$

$$I_{sat} = \frac{\pi}{3}\frac{hc}{\lambda^3\tau_S}. \tag{2}$$

Therefore, the radiative lifetime for SiF in the $A\,^2\Sigma^+$ state is estimated to be 0.23 μs,[20] while the corresponding saturation absorption intensity I_{sat} can be estimated to be on the order of 1.0 mW/cm^2.

III. RESULTS

The high-resolution LIF spectrum of the $A\,^2\Sigma^+$ ($v' = 0$) ← $X\,^2\Pi_{1/2}$ ($v = 0$) transition of SiF has been recorded in the frequency region of 685 488 680–685 687 560 MHz. As shown in Fig. 2(a), a total of 94 fluorescence lines were measured. To facilitate intuitive identification of the transitions, the hyperfine-resolved rotational distribution is classified into six branches: $P_{ee}(J)$, $P_{ff}(J)$, $Q_{fe}(J)$, $Q_{ef}(J)$, $R_{ee}(J)$, and $R_{ff}(J)$. Here, P, Q, and R denote transitions with $\Delta J = J' - J = -1$, 0, and +1, respectively, where J' and J are the total

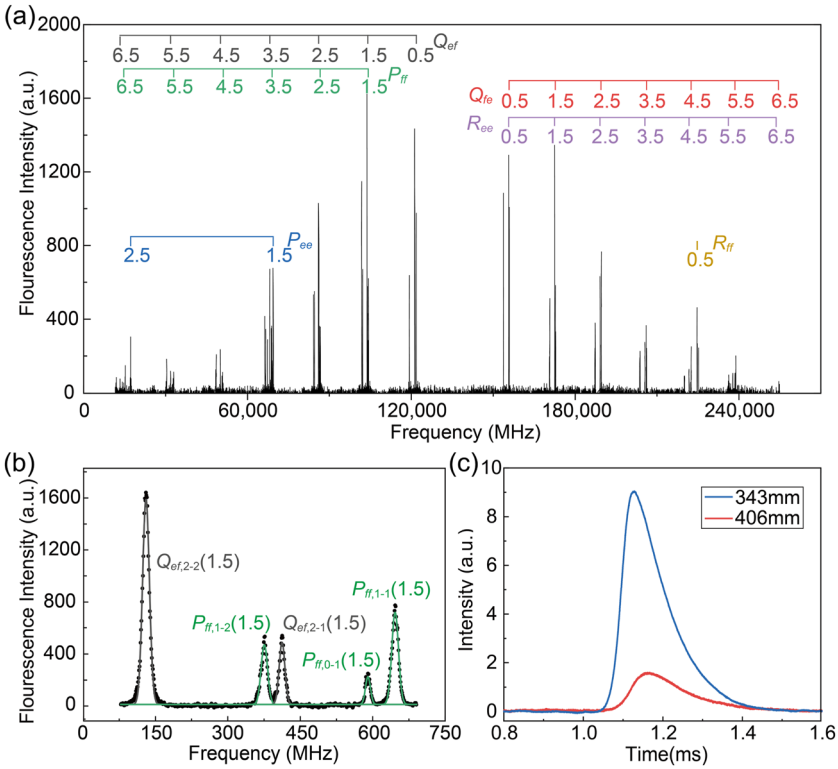

FIG. 2. (a) The LIF spectrum of the $A\,^2\Sigma^+$ ($v' = 0$) ← $X\,^2\Pi_{1/2}$ ($v = 0$) transition of SiF. Different rotational branches are marked in the figure. The x-axis represents the frequency offset referenced to 685 445 440 MHz. (b) A magnified view of the experimental spectrum in the range of 685 549 050–685 549 800 MHz. The x-axis represents the frequency offset referenced to 685 549 050 MHz. (c) Fluorescence profiles of the $Q_{ef,2\text{-}2}(1.5)$ transition recorded separately at 343 and 406 mm downstream from the ablation spot.

angular momentum quantum numbers (excluding nuclear spin) of the upper ($A\ ^2\Sigma^+$) and lower ($X\ ^2\Pi_{1/2}$) electronic states. For those states with total electron spin of $S = 1/2$, the e/f designation is determined by the sign of $q\chi = p_s(-1)^{J-1/2}$, where $p_s = \pm 1$ represents the system parity considering all coordinates without nuclear spin. In this system, the quantum state is labeled by "e" with $q\chi = 1$ and "f" with $q\chi = -1$.[46,49–51] The hyperfine-resolved transitions in this study are assigned as $\Delta J_{q'\chi' q\chi, F'-F}(J)$, where F' and F represent the total angular momentum quantum numbers (including nuclear spin) of the $A\ ^2\Sigma^+$ and $X\ ^2\Pi_{1/2}$ states, respectively. We employed the PGOPHER program[52] to identify and assign transitions. The spectroscopic assignment, including all observed transitions and residuals between the measured and calculated transition frequencies, is presented in Table I, while those notable lines are indicated in Fig. 2(a). In Fig. 2(b), the selected hyperfine-resolved fluorescence spectrum in the range of 685 549 050–685 549 800 MHz (22 867.45–22 867.48 cm^{-1}) involving five peaks originating from $Q_{ef,2\text{-}2}(1.5)$, $P_{ff,1\text{-}2}(1.5)$, $Q_{ef,2\text{-}1}(1.5)$, $P_{ff,0\text{-}1}(1.5)$, and $P_{ff,1\text{-}1}(1.5)$ transitions are displayed. Using a multi-peak least-squares fitting method, the corresponding full width at half maximum (FWHM) was determined to be 8.34, 7.90, 7.02, 8.22, and 6.04 MHz, respectively.

To measure the forward velocity of the buffer gas cooled SiF beam, fluorescence signals corresponding to the $Q_{ef,2\text{-}2}(1.5)$ transition were simultaneously recorded using detectors positioned at 343 and 406 mm downstream from the ablation point (Fig. 1). The forward velocity was calculated by $v = \Delta L/\Delta t$, where ΔL is the distance between the two LIF detection spots and Δt is the time interval between the peaks of the two fluorescence signals.[53] To maximize the signal intensity, experimental parameters were optimized such that a helium flow rate of 2.0 SCCM, a CF_4 flow rate of 0.1 SCCM, and an ablation laser pulse energy of 20 mJ were determined.

TABLE I. The hyperfine-resolved lines of the $A\ ^2\Sigma^+$ ($v' = 0$) ← $X\ ^2\Pi_{1/2}$ ($v = 0$) transition of SiF. The residuals between observed and calculated transition frequencies are presented in parentheses of observed frequency values (Obs.).

Label	Obs. (MHz)	Label	Obs. (MHz)	Label	Obs. (MHz)
$Q_{ef,0\text{-}1}(0.5)$[a]	685 564 720.4(−0.9)	$Q_{ef,5\text{-}6}(5.5)$	685 475 643.9(−4.9)	$Q_{fe,3\text{-}3}(2.5)$	685 634 931.9(31.6)
$Q_{ef,1\text{-}1}(0.5)$	685 566 714.2(12.9)	$Q_{ef,5\text{-}5}(5.5)$	685 475 864.0(−0.5)	$R_{ee,4\text{-}3}(3.5)$	685 649 022.0(−10.0)
$Q_{ef,1\text{-}0}(0.5)$	685 567 188.8(23.5)	$Q_{ef,6\text{-}6}(5.5)$	685 477 271.1(0.8)	$R_{ee,4\text{-}4}(3.5)$	685 649 154.8(−12.7)
$Q_{ef,1\text{-}2}(1.5)$	685 547 297.2(−0.3)	$P_{ff,5\text{-}6}(5.5)$	685 477 985.2(1.8)	$R_{ee,5\text{-}4}(3.5)$	685 650 855.3(10.6)
$Q_{ef,2\text{-}2}(1.5)$	685 549 193.6(7.8)	$P_{ff,5\text{-}5}(5.5)$	685 478 190.8(−8.3)	$Q_{fe,4\text{-}3}(3.5)$	685 651 288.4(−8.1)
$P_{ff,1\text{-}2}(1.5)$	685 549 437.1(7.0)	$P_{ff,4\text{-}5}(5.5)$	685 478 449.6(−10.4)	$Q_{fe,4\text{-}4}(3.5)$	685 651 430.1(−1.9)
$Q_{ef,2\text{-}1}(1.5)$	685 549 480.4(12.6)	$P_{ee,2\text{-}2}(2.5)$	685 462 546.5(−19.6)	$Q_{fe,3\text{-}3}(3.5)$	685 651 496.3(−4.1)
$P_{ff,0\text{-}1}(1.5)$	685 549 662.3(10.9)	$P_{ee,2\text{-}3}(2.5)$	685 462 670.3(−20.0)	$Q_{fe,3\text{-}4}(3.5)$	685 651 637.6(1.7)
$P_{ff,1\text{-}1}(1.5)$	685 549 720.3(8.3)	$O_{fe,1\text{-}2}(2.5)$	685 462 790.0(−20.3)	$R_{ee,5\text{-}4}(4.5)$	685 665 300.4(−1.5)
$Q_{ef,1\text{-}1}(1.5)$	685 547 589.4(10.0)	$P_{ee,1\text{-}2}(2.5)$	685 460 664.2(−13.6)	$R_{ee,5\text{-}5}(4.5)$	685 665 448.3(4.5)
$Q_{ef,2\text{-}3}(2.5)$	685 529 684.3(9.0)	$P_{ff,5\text{-}6}(6.5)$	685 460 175.8(−19.7)	$R_{ee,6\text{-}5}(4.5)$	685 667 049.1(−16.1)
$Q_{ef,2\text{-}2}(2.5)$	685 529 923.0(2.9)	$P_{ff,6\text{-}7}(6.5)$	685 459 648.6(-22.9)	$Q_{fe,5\text{-}4}(4.5)$	685 667 621.2(−15.3)
$Q_{ef,3\text{-}3}(2.5)$	685 531 468.3(−16.5)	$Q_{ef,7\text{-}7}(6.5)$	685 458 809.2(−18.1)	$Q_{fe,5\text{-}5}(4.5)$	685 667 767.2(−11.1)
$Q_{ef,3\text{-}2}(2.5)$	685 531 716.6(−13.0)	$Q_{ef,6\text{-}7}(6.5)$	685 457 240.4(−15.1)	$S_{ef,2\text{-}1}(0.5)$	685 667 847.3(−10.4)
$P_{ff,2\text{-}3}(2.5)$	685 531 825.4(−12.5)	$Q_{ef,6\text{-}6}(6.5)$	685 457 451.8(−16.3)	$Q_{fe,4\text{-}4}(4.5)$	685 667 887.8(−9.6)
$P_{ff,2\text{-}2}(2.5)$	685 532 075.7(−7.0)	$R_{ee,1\text{-}1}(0.5)$	685 599 111.6(−19.3)	$R_{ff,2\text{-}1}(0.5)$	685 670 005.2(−15.1)
$P_{ff,1\text{-}2}(2.5)$	685 532 139.8(−4.7)	$R_{ee,2\text{-}1}(0.5)$	685 601 006.3(−12.9)	$R_{ff,1\text{-}1}(0.5)$	685 670 064.3(−17.8)
$Q_{ef,3\text{-}4}(3.5)$	685 511 876.8(17.7)	$Q_{fe,0\text{-}1}(0.5)$	685 601 193.2(−9.7)	$R_{ff,1\text{-}0}(0.5)$	685 670 539.6(−6.5)
$Q_{ef,3\text{-}3}(3.5)$	685 512 083.0(−5.1)	$Q_{fe,1\text{-}0}(0.5)$	685 601 239.2(−8.6)	$R_{ee,6\text{-}5}(5.5)$	685 681 390.6(13.3)
$P_{ee,0\text{-}1}(1.5)$[a]	685 512 783.3(1.5)	$Q_{fe,1\text{-}1}(0.5)$	685 601 255.4(−8.1)	$R_{ee,6\text{-}6}(5.5)$	685 681 538.1(15.1)
$Q_{ef,4\text{-}4}(3.5)$	685 513 600.3(1.6)	$R_{ee,2\text{-}1}(1.5)$	685 615 927.0(8.8)	$Q_{ee,7\text{-}6}(5.5)$	685 683 102.2(7.5)
$P_{ff,3\text{-}4}(3.5)$	685 514 075.0(9.1)	$R_{ee,2\text{-}2}(1.5)$	685 616 026.3(7.5)	$Q_{fe,6\text{-}5}(5.5)$	685 683 814.4(21.1)
$P_{ff,3\text{-}3}(3.5)$	685 514 302.7(7.7)	$R_{ee,3\text{-}2}(1.5)$	685 617 832.9(4.6)	$Q_{fe,6\text{-}6}(5.5)$	685 683 961.8(22.8)
$P_{ff,2\text{-}3}(3.5)$	685 514 445.2(11.3)	$Q_{fe,2\text{-}1}(1.5)$	685 618 073.9(−6.9)	$Q_{fe,5\text{-}5}(5.5)$	685 684 132.7(28.0)
$P_{ee,1\text{-}1}(1.5)$	685 514 769.8(8.0)	$Q_{fe,1\text{-}1}(1.5)$	685 618 138.1(−4.5)	$R_{ee,7\text{-}6}(6.5)$	685 697 247.5(−9.4)
$P_{ee,1\text{-}2}(1.5)$	685 514 866.7(4.3)	$Q_{fe,2\text{-}2}(1.5)$	685 618 176.2(−5.2)	$R_{ee,7\text{-}7}(6.5)$	685 697 405.9(0.9)
$Q_{ef,4\text{-}5}(4.5)$	685 493 841.6(−8.5)	$Q_{fe,1\text{-}2}(1.5)$	685 618 232.1(−11.1)	$R_{ee,8\text{-}7}(6.5)$	685 698 946.6(14.4)
$Q_{ef,4\text{-}4}(4.5)$	685 494 058.3(−12.4)	$R_{ee,3\text{-}2}(2.5)$	685 632 593.9(24.6)	$Q_{fe,7\text{-}7}(6.5)$	685 699 917.5(4.9)
$Q_{ef,5\text{-}5}(4.5)$	685 495 533.9(6.6)	$R_{ee,3\text{-}3}(2.5)$	685 632 717.3(23.8)	$Q_{fe,6\text{-}6}(6.5)$	685 700 119.9(−1.0)
$P_{ff,4\text{-}5}(4.5)$	685 496 115.3(0.7)	$R_{ee,4\text{-}3}(2.5)$	685 634 462.7(29.6)	$Q_{fe,7\text{-}6}(6.5)$	685 699 762.6(−1.9)
$P_{ff,4\text{-}4}(4.5)$	685 496 331.2(−4.0)	$Q_{fe,3\text{-}2}(2.5)$	685 634 803.5(27.4)		
$P_{ff,3\text{-}4}(4.5)$	685 496 542.7(3.6)	$Q_{fe,2\text{-}2}(2.5)$	685 634 946.5(31.5)		

[a]The transition lines for laser cooling.

Under these conditions, the forward velocity of the SiF beam was measured to be 239 ± 12 m/s, which is close to the measured velocities of SrF,[54] BaF,[55] and PbF[46] of 140 ± 21, 184 ± 15, and 223 ± 17 m/s. It should be noted that the forward velocity is influenced by many factors, including the buffer gas temperature, the flow rates of He and the reactant CF_4, the ablation laser intensity, and even the design and geometry of the source chamber.

IV. DISCUSSION

For the ground $X\ ^2\Pi_{1/2}$ state of SiF, the energy level structure is described using the Hund's case (a) angular momentum coupling scheme. The corresponding effective Hamiltonian is given as

$$H_{eff} \approx H_{rso} + H_{hfs}, \tag{3}$$

where H_{rso} includes the rotational, spin–orbit coupling, Λ-type doubling, and spin–rotation Hamiltonians, while H_{hfs} denotes the hyperfine interaction Hamiltonian. The basis functions employed are symmetry-adapted Hund's case (a) functions, given by

$$\left|^2\Pi_\Omega J\pm\right\rangle = \frac{\left[\left|J\Omega S\Sigma\Lambda\right\rangle \pm (-1)^{J-S}\left|J-\Omega S-\Sigma-\Lambda\right\rangle\right]}{\sqrt{2}}. \tag{4}$$

The matrix elements of H_{eff} in the $X\ ^2\Pi_{1/2}$ state have been given in previous studies.[27,56] To measure the hyperfine transitions, the corresponding energy levels of the upper $A\ ^2\Sigma^+$ state need to be investigated. Here, the $A\ ^2\Sigma^+$ state is simulated within the Hund's case (b) coupling scheme. In this case, the electron spin S couples with the rotational angular momentum N to form the total angular momentum $J = N + S$. The effective Hamiltonian includes the molecular rotational term H_R, the spin–rotation coupling term H_{SR}, and the hyperfine interaction term H_{hfs}, which are expressed as[57]

$$H'_{eff} = H'_R + H'_{SR} + H'_{hfs} = B\boldsymbol{N}^2 - D\boldsymbol{N}^4 + \gamma\boldsymbol{N}\cdot\boldsymbol{S} + H'_{hfs}, \tag{5}$$

where B, D, and γ represent the rotational constant, the centrifugal distortion constant, and the spin–rotation constant, respectively. In the Hund's case (b) basis, the energy of the $A\ ^2\Sigma^+$ state, excluding the hyperfine interaction term, can be expressed as

$$\begin{aligned} E_R+E_{SR} = {} & BN(N+1) - D[N(N+1)]^2 \\ & + \gamma(-1)^{N+J+s}\sqrt{S(S+1)(2S+1)} \\ & \times\sqrt{N(N+1)(2N+1)}\begin{Bmatrix} S & N & J \\ N & S & 1 \end{Bmatrix} + T_{00}, \end{aligned} \tag{6}$$

and the hyperfine interaction Hamiltonian H_{hfs} for the $A\ ^2\Sigma^+$ state is given by[58]

$$H'_{hfs} = b_F T^1(\hat{I})T^1(\hat{S}) + cT^1_{q=0}(\hat{I})T^1_{q=0}(\hat{S}) + C_n T^1(\hat{I})T^1(\hat{N}). \tag{7}$$

Here, the Fermi contact constant is given by $b_F = b + c/3$, where b and c denote the hyperfine constant and the dipole–dipole interaction constant, respectively, as defined within the Frosch and Foley formalism.[59] The nuclear spin–rotational coupling constant C_n is negligibly small and is therefore omitted in the calculations.

Based on the hyperfine-resolved molecular spectra, the previously reported $X\ ^2\Pi_{1/2}$ state parameters[27] were fixed in the PGOPHER program,[52] and the molecular constants of the $A\ ^2\Sigma^+$ state were determined using an iterative least-squares fitting. The derived fine and hyperfine constants, including the rotational constant (B_0), the centrifugal distortion constant (D_0), the spin–orbit coupling constant (A_0) and its centrifugal distortion parameter (A_J), are summarized in Table II, resulting in a mean deviation of 13.8 MHz. Note that the value of A_0 was fixed at 161.88 cm^{-1}.[19,27] Furthermore, the parameters p_0 and q_0 are Λ-doubling constants; a, b, c, and d represent the hyperfine interaction constants; γ is the spin–rotation coupling constant; and T_{00} denotes the energy of the $A\ ^2\Sigma^+$ state at $v = 0$ and $J = 0$. For the $X\ ^2\Pi_{1/2}$ state, the γ value was neglected at this stage due to its correlation with A_J.[60,61] We employed the effective Hamiltonian theory to calculate the hyperfine-resolved level structures of the $X\ ^2\Pi_{1/2}$ and $A\ ^2\Sigma^+$ states, thereby providing a clearer spectral framework for subsequent laser cooling analysis. The effective Hamiltonian H_{eff} and the basis set $|F, I, J, M_F, p_s\rangle$ are depicted within the Hund's case (a) coupling framework in our previous article.[59,62] These molecular constants in Table II were then employed to solve and analyze the spin–rotation and hyperfine interactions in the $A\ ^2\Sigma^+$ $(v' = 0) \leftarrow X\ ^2\Pi_{1/2}$ $(v = 0)$ transition with the corresponding hyperfine energy level structures of $X\ ^2\Pi_{1/2}$ $(v = 0)$ and $A\ ^2\Sigma^+$ $(v' = 0)$ in the absence of external fields (Fig. 3).

Recently, SiF has been tentatively identified as a promising candidate for laser cooling and precision measurement. The $A\ ^2\Sigma^+$ $(v' = 0) \leftarrow X\ ^2\Pi_{1/2}$ $(v = 0)$ transition of SiF exhibits a large Einstein A coefficient ($A_{00} = 1.45 \times 10^6$) and a highly diagonal vibrational branching ratio R_{00} of 0.994. These favorable optical properties yield a Doppler temperature of 5.7 μK and a recoil temperature of 2.12 μK, indicating that SiF could be cooled to the ultracold regime. Such characteristics support the theoretical feasibility of implementing a

TABLE II. The fine and hyperfine constants (in units of MHz) for the $X\ ^2\Pi$ and $A\ ^2\Sigma^+$ states of SiF. For the $X\ ^2\Pi_{1/2}$ state, the numbers in parentheses denote three standard deviations in the last two digits, whereas for the $A\ ^2\Sigma^+$ state, they represent one standard deviation in the last two digits.

	$X\ ^2\Pi_{1/2}$[a]	$A\ ^2\Sigma^+$
B_0	17 350.275 2 (63)	17 193.39 (29)
D_0	0.031 88 (13)	0.037 9 (55)
A_0	4 853 040.310 104[b]	⋯
A_J	1.630 6 (42)	⋯
$p_0 + 2q_0$	−90.19 (17)	⋯
q_0	−1.26 (29)	⋯
a	312.35 (60)	⋯
b	127 (16)	1 884.8 (53)
c	−175 (16)	286 (12)
d	359.0 (33)	⋯
b_F	⋯	1980.1 (66)[c]
γ	⋯	−179.52 (99)
T_{00}	⋯	683 174 454.2 (27)

[a] Converted from Ref. 27.
[b] A_0 is fixed to 161.88 cm^{-1} based on Refs. 19 and 27.
[c] Calculated from experimentally determined parameters.

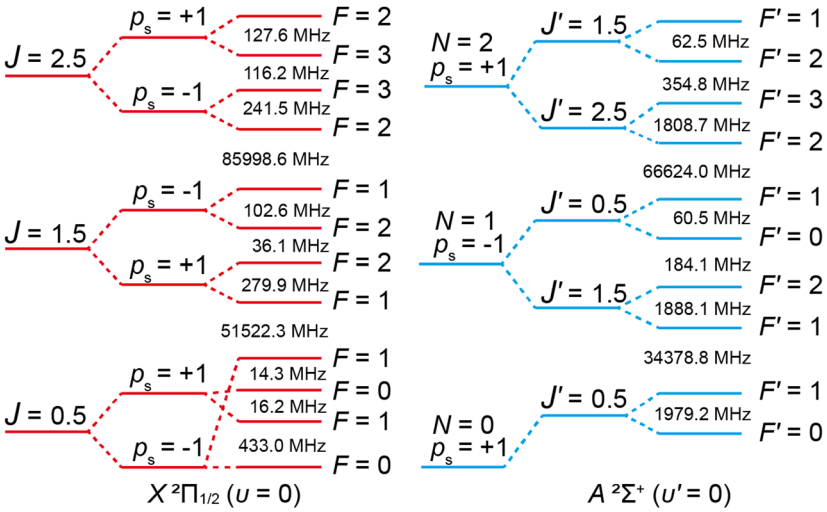

FIG. 3. The energy level structures of $X\ ^2\Pi_{1/2}$ ($v' = 0$) and $A\ ^2\Sigma^+$ ($v' = 0$) states of SiF in the absence of an external electric field.

closed laser cooling cycle. Although Xia *et al.*[43] proposed a two-laser cooling strategy for SiF, their study did not account for the influence of the hyperfine structure of the $^2\Pi$ ground state. Here, with the well-defined hyperfine structures for both ground $X\ ^2\Pi_{1/2}$ ($v = 0$) and upper $A\ ^2\Sigma^+$ ($v' = 0$) states, the suitability of SiF for laser cooling is further investigated. The pumping schemes for the laser cooling experiment generally rely on rotationally closed transitions, which require careful consideration of both excitation and decay processes. To date, the $A\ ^2\Pi_{1/2} \leftarrow X\ ^2\Sigma^+$ transition represents the most commonly used transition in the laser cooling strategy for diatomic molecules. For these experiments, the levels of $J' = 0.5$ and $p_s = +1$ generally exhibit near-degeneracy in hyperfine states of $F' = 0$ and $F' = 1$ in the excited $A\ ^2\Pi_{1/2}$ state. Consequently, a conventional optical cycling scheme must simultaneously address both $F' = 0$ and $F' = 1$ states within the $J' = 0.5$, $p_s = +1$ manifold to maintain closure. However, in the case of SiF, these two hyperfine levels—$J' = 0.5$, $p_s = +1$, $F' = 0$, and $F' = 1$—are separated by 1979.2 MHz, as shown in Fig. 3. This large splitting greatly simplifies the optical cycling scheme, enabling an effectively closed transition by driving only the $F' = 0$ within the $J' = 0.5$, $p_s = +1$ manifold.

According to our experimental results, only $Q_{ef,0\text{-}1}(0.5)$ [$A(J' = 0.5, e, F' = 0) \leftarrow X(J = 0.5, f, F = 1)$] and $P_{ee,0\text{-}1}(1.5)$ [$A(J' = 0.5, e, F' = 0) \leftarrow X(J = 1.5, e, F = 1)$] transitions are observed for those transitions involving $A(J' = 0.5, e, F' = 0)$. The $Q_{ef,0\text{-}0}(0.5)$ transition is missing, which agrees with the corresponding calculated transition dipole moments (supplementary material, Table S1). The transitions in Table I are organized by transition frequency, with $Q_{ef,0\text{-}1}(0.5)$ and $P_{ee,0\text{-}1}(1.5)$ labeled as "a." As shown in Table I, these adjacent lines are well resolved and notably isolated from neighboring transitions by at least 700 MHz. These results indicate that no dark states interfere with these optical cycling transitions, which are also confirmed by our PGOPHER simulation. For the $Q_{ef,0\text{-}1}(0.5)$ and $P_{ee,0\text{-}1}(1.5)$ transitions, the frequency separation is measured to be 51 937.1 MHz. This large interval precludes the generation of both frequencies via sideband modulation using a commercial electro-optic modulator (EOM). Therefore, two independent laser sources are necessary to optically pump these transitions. Note that the present analysis focuses only on the $A^2\Sigma^+$ ($v' = 0$) $\leftarrow X\ ^2\Pi$ ($v = 0$) transition. For the repumping transition of $A\ ^2\Sigma^+$ ($v' = 0$) $\leftarrow X\ ^2\Pi_{1/2}$ ($v = 1$), two more 455.5 nm lasers are needed. With the development of the buffer gas cooling technique, dense molecular beams with low forward velocity have been generated. Considering both the $A\ ^2\Sigma^+$ ($v' = 0$) $\leftarrow X\ ^2\Pi_{1/2}$ ($v = 0$) and $A\ ^2\Sigma^+$ ($v' = 0$) $\leftarrow X\ ^2\Pi_{1/2}$ ($v = 1$) transitions, the number of photons scattered per molecule is estimated to be about 1.1×10^3, which can already slow the molecules down to the capture velocity of a three-dimensional MOT of 10 m/s.[43] Therefore, a minimum of four lasers is required to realize a closed optical cycle: two primary lasers to drive the main transitions within $A\ ^2\Sigma^+$ ($v' = 0$) $\leftarrow X\ ^2\Pi_{1/2}$ ($v = 0$) and at least two additional repump lasers to address population leakage into the transition of $A^2\Sigma^+$ ($v' = 0$) $\leftarrow X\ ^2\Pi_{1/2}$ ($v = 1$) and other off-resonant levels. It should be noted that the spin–orbit coupling in the $X\ ^2\Pi$ state leads to a splitting into $X\ ^2\Pi_{1/2}$ and $X\ ^2\Pi_{3/2}$ components; a comparable number of lasers might be necessary to address leakages from the $A\ ^2\Sigma^+ \leftarrow X\ ^2\Pi_{3/2}$ transition. Therefore, more experimental and theoretical investigations for the $^2\Pi_{3/2}$ state are needed in the potential laser cooling experiment using SiF.

V. CONCLUSIONS

To summarize, we have performed high-resolution laser-induced fluorescence spectroscopy studies of the $A\ ^2\Sigma^+$ ($v' = 0$) $\leftarrow X\ ^2\Pi_{1/2}$ ($v = 0$) transition of SiF molecules produced with the buffer gas cooling technique. A total of 94 hyperfine-resolved spectra were recorded and analyzed, with a frequency uncertainty of 13.8 MHz. This analysis enabled the determination of precise molecular constants for the $A\ ^2\Sigma^+$ state, including the hyperfine constant b and the dipole–dipole interaction constant c for low-J levels. Using the fitted molecular constants, we evaluated the effective Hamiltonian matrix elements to resolve the hyperfine structure of the $X\ ^2\Pi_{1/2}$ and $A\ ^2\Sigma^+$ states, thereby providing a spectroscopic foundation for SiF-related studies and prospective laser cooling applications. Our analysis further identifies two rotationally closed transitions relevant

to optical cycling in the $A\,^2\Sigma^+$ ($v' = 0$) ← $X\,^2\Pi_{1/2}$ ($v = 0$) transition. However, additional transitions, such as $A^2\Sigma^+$ ($v' = 0$) ← $X\,^2\Pi_{1/2}$ ($v = 1$) and $A\,^2\Sigma^+$ ← $X\,^2\Pi_{3/2}$, must be incorporated to repump population leakage and improve the overall cooling efficiency. Consequently, a minimum of four laser frequencies is required, which presents a considerable experimental challenge. These findings establish a robust spectroscopic foundation for evaluating SiF as a candidate for direct laser cooling, with implications for its applications in quantum control, precision measurement, and astrophysical and plasma environments.

SUPPLEMENTARY MATERIAL

The supplementary material contains the hyperfine branching ratios for the $Q_{ef,0\text{-}0}(0.5)$ transition.

ACKNOWLEDGMENTS

We acknowledge the support from the National Natural Science Foundation of China (Grant Nos. 12274140, 12034008, 12250003, 92461301, 12473025, 12304310, 12174247, 92265209, 2574379, and 12595341), the Xinjiang Tianchi Talent Program (2023), the Natural Science Foundation of Xinjiang Uygur Autonomous Region (Grant No. 2024D01E37), the Program for Professor of Special Appointment (Eastern Scholar) at Shanghai Institutions of Higher Learning, the Young Top-Notch Talent Support Program of Shanghai, and the Shanghai Natural Science Foundation (Grant No. 22ZR1421400).

AUTHOR DECLARATIONS

Conflict of Interest

The authors have no conflicts to disclose.

Author Contributions

Jie Ma: Investigation (equal); Methodology (equal); Writing – original draft (equal). **Yuxi Feng**: Investigation (equal). **Yemin Pan**: Investigation (equal). **Shanwu Wang**: Investigation (equal). **Rui Li**: Investigation (equal). **Zesen Wang**: Investigation (equal). **Shunyong Hou**: Investigation (equal). **Xilin Bai**: Investigation (equal). **Xiaohu Li**: Investigation (equal). **Liang Xu**: Investigation (equal). **Xingjia Li**: Investigation (equal). **Zhenghai Yang**: Conceptualization (equal); Investigation (equal); Methodology (equal); Validation (equal); Writing – review & editing (equal). **Jianping Yin**: Investigation (equal). **Tao Yang**: Conceptualization (equal); Formal analysis (equal); Investigation (equal); Project administration (equal); Supervision (equal); Validation (equal); Writing – review & editing (equal).

DATA AVAILABILITY

The data that support the findings of this study are available from the corresponding authors upon reasonable request.

REFERENCES

[1] P. Stenberg *et al.*, J. Phys. Chem. C **121**, 2711 (2017).
[2] B. J. Garrison and W. A. Goddard III, J. Chem. Phys. **87**, 1307 (1987).
[3] R. Walkup *et al.*, Appl. Phys. Lett. **45**, 372 (1984).
[4] J. Zhang, K. L. Williams, and E. R. Fisher, J. Phys. Chem. A **107**, 593 (2003).
[5] K. L. Williams and E. R. Fisher, J. Vac. Sci. Technol. A **21**, 1024 (2003).
[6] K. G. McKendrick, J. Chem. Soc., Faraday Trans. **94**, 1921 (1998).
[7] N. A. Jackson, C. J. Randall, and K. G. McKendrick, Chem. Phys. **233**, 45 (1998).
[8] M.-T. Lee *et al.*, Phys. Rev. A **66**, 062703 (2002).
[9] R. W. Nicholls, Annu. Rev. Astron. Astrophys. **15**, 197 (1977).
[10] K. Nagarajan *et al.*, Astron. Astrophys. Suppl. Ser. **129**, 157 (1998).
[11] R. A. King, V. S. Mastryukov, and H. F. Schaefer III, J. Chem. Phys. **105**, 6880 (1996).
[12] P. O'Hare, J. Chem. Phys. **59**, 3842 (1973).
[13] P. O'Hare and A. C. Wahl, J. Chem. Phys. **55**, 666 (1971).
[14] R. Kishi *et al.*, J. Chem. Phys. **108**, 8039 (1998).
[15] S. P. Frigo, J. K. Simons, and R. A. Rosenberg, J. Chem. Phys. **103**, 10366 (1995).
[16] E. R. Fisher, B. L. Kickel, and P. B. Armentrout, J. Phys. Chem. **97**, 10204 (1993).
[17] N. O. J. Malcolm and D. L. Yeager, J. Chem. Phys. **113**, 8 (2000).
[18] J. W. C. Johns and R. F. Barrow, Proc. Phys. Soc. **71**, 476 (1958).
[19] R. W. Martin and A. J. Merer, Can. J. Phys. **51**, 634 (1973).
[20] S. J. Davis and S. G. Hadley, Phys. Rev. A **14**, 1146 (1976).
[21] K. Wang and V. McKoy, J. Chem. Phys. **97**, 5489 (1992).
[22] C. W. Watson and K. G. McKendrick, Chem. Phys. **187**, 87 (1994).
[23] J. M. Robbe *et al.*, J. Mol. Spectrosc. **112**, 228 (1985).
[24] H. Bredohl *et al.*, J. Mol. Spectrosc. **129**, 232 (1988).
[25] F. Remy *et al.*, J. Mol. Spectrosc. **152**, 131 (1992).
[26] M. Ebben, M. Versluis, and J. J. ter Meulen, J. Mol. Spectrosc. **149**, 329 (1991).
[27] M. Tanimoto *et al.*, J. Mol. Spectrosc. **100**, 205 (1983).
[28] R. H. Petrmichl, K. A. Peterson, and R. C. Woods, J. Chem. Phys. **89**, 5454 (1988).
[29] K. Tanaka, Y. Akiyama, and T. Tanaka, J. Mol. Spectrosc. **137**, 55 (1989).
[30] J. M. Robbe, J. Mol. Spectrosc. **112**, 223 (1985).
[31] D. H. Shi *et al.*, Int. J. Quantum Chem. **112**, 2615 (2012).
[32] D. Wu *et al.*, Front. Phys. **20**, 032201 (2025).
[33] S. Truppe *et al.*, Phys. Rev. A **100**, 052513 (2019).
[34] V. Zhelyazkova *et al.*, Phys. Rev. A **89**, 053416 (2014).
[35] J. F. Barry *et al.*, Nature **512**, 286 (2014).
[36] Z. Zeng *et al.*, Phys. Rev. Lett. **133**, 143404 (2024).
[37] J. Lim *et al.*, Phys. Rev. Lett. **120**, 123201 (2018).
[38] T. A. Isaev, S. Hoekstra, and R. Berger, Phys. Rev. A **82**, 052521 (2010).
[39] Z. Yang *et al.*, Phys. Rev. A **99**, 032502 (2019).
[40] T. S. Roussy *et al.*, Science **381**, 46 (2023).
[41] J. J. Hudson *et al.*, Nature **473**, 493 (2011).
[42] C. Zhu *et al.*, J. Chem. Phys. **157**, 084307 (2022).
[43] W. Xia *et al.*, Chem. Phys. **485**, 29 (2017).
[44] T. Prohaska *et al.*, Pure Appl. Chem. **94**, 573 (2022).
[45] K. L. Williams *et al.*, Chem. Phys. Lett. **323**, 137 (2000).
[46] Z. Wang *et al.*, Spectrochim. Acta, Part A **329**, 125508 (2025).
[47] W. Demtröder, NASA STI/Recon Tech. Rep. A 82, 1981, p. 12273.
[48] D. A. Steck, Rubidium 85 D Line Data (2001); https://www.steck.us/alkalidata/rubidium85numbers.pdf.
[49] P. Sivakumar *et al.*, Mol. Phys. **108**, 927 (2010).
[50] I. Kopp and J. T. Hougen, Can. J. Phys. **45**, 2581 (1967).
[51] J. Brown *et al.*, J. Mol. Spectrosc. **55**, 500 (1975).
[52] C. M. Western, J. Quant. Spectrosc. Radiat. Transfer **186**, 221 (2017).
[53] S. Truppe *et al.*, J. Mod. Opt. **65**, 648 (2018).
[54] J. F. Barry, E. S. Shuman, and D. DeMille, Phys. Chem. Chem. Phys. **13**, 18936 (2011).
[55] J. W. F. van Hofslot *et al.*, Commun. Phys. **9**, 24 (2026).

[56]Y. Endo, S. Saito, and E. Hirota, J. Mol. Spectrosc. **92**, 443 (1982).
[57]J. M. Brown and A. Carrington, *Rotational Spectroscopy of Diatomic Molecules* (Cambridge University Press, Cambridge, 2003).
[58]T. Chen, W. Bu, and B. Yan, Phys. Rev. A **94**, 063415 (2016).
[59]R. A. Frosch and H. M. Foley, Phys. Rev. **88**, 1337 (1952).
[60]J. M. Brown and J. K. G. Watson, J. Mol. Spectrosc. **65**, 65 (1977).
[61]S. Jackson *et al.*, Phys. Rev. A **110**, 042808 (2024).
[62]Z. Wang *et al.*, J. Quant. Spectrosc. Radiat. Transfer **347**, 109658 (2025).